Two-Dimensional SPICE-Linked Multiresolution Impedance Method for Low-Frequency Electromagnetic Interactions

Michael Eberdt, Patrick K. Brown, and Gianluca Lazzi*, *Senior Member, IEEE*

***Abstract*—A multiresolution impedance method for the solution of low-frequency electromagnetic interaction problems typically encountered in bioelectromagnetics is presented. While the impedance method in its original form is based on the discretization of the scattering objects into equal-sized cells, our formulation decreases the number of unknowns by using an automatic mesh generation method that does not yield equal-sized cells in the modeling space. Results indicate that our multiresolution mesh generation scheme can provide a 50%–80% reduction in cell count, providing new opportunities for the solution of low-frequency bioelectromagnetic problems that require a high level of detail only in specific regions of the modeling space. Furthermore, linking the mesh generator to a circuit simulator such as SPICE permits the addition of arbitrarily complex passive and active circuit elements to the generated impedance network, opening the door to significant advances in the modeling of bioelectromagnetic phenomena.**

***Index Terms*—Dosimetry, electromagnetic modeling, induced fields, numerical modeling.**

I. Introduction

THE impedance method was introduced in 1984 by Gandhi *et al.* [1] as a simulation method suitable for quasi-static electromagnetic radiation problems that arise in the field of bioelectromagnetics. It is a conceptually simple technique for computing the currents induced in objects by a low-frequency electromagnetic stimulus. The method is attractive for biomedical simulations because of its relative simplicity, which is retained even when applied to nontrivial problems involving spatially varying magnetic sources, or oddly shaped heterogeneous objects such as the human body.

As with most simulation methods involving complex objects, the physical model must be discretized into elementary cells having a size and shape that are amenable to the mathematics of the simulation method. In the impedance method, the cells are simply rectangles in two-dimensional (2-D) problems and rectangular polyhedrons in three-dimensional (3-D) problems. After the physical model is discretized into a mesh, or grid, of these simple cells, an impedance network is constructed using lumped impedances derived from the material properties of each cell. The electromagnetic stimulus present in the physical model is realized as voltages induced around loops, or currents injected into nodes, of the network. Standard circuit analysis techniques are then used to obtain the branch currents within the impedance network. Finally, the correspondence between impedances in the network and cells in the discretized model is used to transform the branch currents into values of current density with magnitude and direction in the physical model.

Traditionally, a uniform grid is used—all cells in the discretized model are identical in size and shape. The use of a uniform grid permits a very straightforward, space-efficient software implementation of the method. However, the number of cells and, thus, the number of branch currents to be solved for, is determined by the smallest geometric feature that must be accurately discretized. As the overall model dimensions become large relative to the smallest feature within the model, the impedance network to be analyzed can become extremely large. For example, a 1-mm resolution, full-body model of an adult man is available [2]. It contains more than 370 000 000 cells, yet many physical details of the human body remain inaccurately modeled, if not completely lost, at that resolution. Improving the resolution by a factor of two would result in an eightfold increase in cells in the uniform grid. However, even at 1-mm resolution, such a model already represents a nontrivial computational task for today's fast, memory-laden machines.

In 1983, Armitage *et al.* [3] introduced a simulation method that is essentially the dual of the impedance method. In that method, the unknowns in the discretized model are voltages rather than currents, and the passive network components are admittances rather than impedances. To obtain sufficient accuracy in the solution, they adopted a technique of selective mesh refinement. After the entire model was simulated at the coarsest resolution, a portion of the model was subdivided to double the resolution. Around the perimeter of the subdivided region, values from the previous simulation were interpolated to twice the spatial density and employed as boundary conditions, and the subdivided portion of the model was simulated again. This resolution enhancement was then reapplied to a portion of the already-subdivided region. This is the type of localized resolution enhancement that we seek in principle. However, it would be highly desirable to eliminate both the need to perform multiple solving steps and the need to explicitly specify the boundaries of various mesh resolutions.

More recently, Dimbylow [4] has employed the scalar potential finite difference (SPFD) method [5], [6] as an alternative

Manuscript received July 10, 2002; revised December 27, 2002. *Asterisk indicates corresponding author.*

M. Eberdt was with the Computer Science Department, North Carolina State University, Raleigh, NC 27691-7914 USA.

P. K. Brown is with the Electrical and Computer Engineering Department, North Carolina State University, Raleigh, NC 27695-7914 USA.

*G. Lazzi is with the Electrical and Computer Engineering Department, North Carolina State University, EGRC Box 7914, Raleigh, NC 27695-7914 USA (e-mail: lazzi@eos.ncsu.edu).

Digital Object Identifier 10.1109/TBME.2003.813534

mathematical formulation for problems in which the impedance method is applicable. The advantage of the SPFD method here is that it replaces a vector computation with a scalar one, significantly reducing the number of unknowns to be solved. However, a useful feature of the impedance method is the ability to augment the basic impedance network using familiar lumped circuit elements such as voltage or current sources, or arbitrarily complex lumped elements of known voltage–current relation. This can be accomplished by using the impedance network derived from the biological body as input to a circuit simulator such as SPICE. With the SPFD method, this flexibility is lost since one is no longer working with an impedance network.

In the case we describe now, we have retained the basic mathematical foundation of the original impedance method because of its flexibility with regard to material configurations and applied stimuli. To decrease the computational burden of the method, we have adapted it to a multiresolution (that is, nonuniform) discretization. The automated meshing scheme described herein requires no intervention from the user, and only a single linear system needs to be solved.

The remainder of this paper is organized as follows: Section II describes our implementation of a multiresolution mesh generation scheme; Section III explains how current density is computed; Section IV addresses the link with SPICE, Section V examines results obtained with multiresolution meshes, and Section VI addresses extension of our method to three dimensions.

II. Multiresolution Meshing

We now describe a method of multiresolution mesh generation for 2-D problems. (The extension of the method to three dimensions is conceptually straightforward) We will use the following terminology.

- A *unit cell* is a 1×1 cell. These dimensionless "grid units" correspond to the smallest resolvable feature size in a mesh. The elements of any uniform mesh are implicitly unit cells.
- A *border* is a property that is associated with an edge or corner of a unit cell, and it serves as a marker. Borders are used to represent all material interfaces, but we may define additional borders anywhere in the mesh we wish to force unit cell resolution.
- A *border cell* is a unit cell that has a border associated with any of its edges or corners. Only unit cells may be border cells.
- A *region* is an enclosed area defined by one or more borders. A region is not necessarily homogeneous; other regions may be embedded within.

The mathematical formulation of the impedance method does not require all cells to be of uniform size, nor does it require cell faces to be rectangular. However, rectangular cell faces are highly desirable because they permit us to model currents and material properties in terms of orthogonal components, which greatly simplify the calculation of the lumped impedances for the impedance network. Thus, we attempt to reduce the size of the linear system by utilizing a variety of rectangular cells within the mesh. Our basic approach is to utilize the smallest cells along the boundaries that separate different materials, and around localized electromagnetic sources, because these are the places where the current density can change most abruptly. As we move farther away from the regions at which there may be abrupt and significant disturbances in current density, we utilize progressively larger cells.

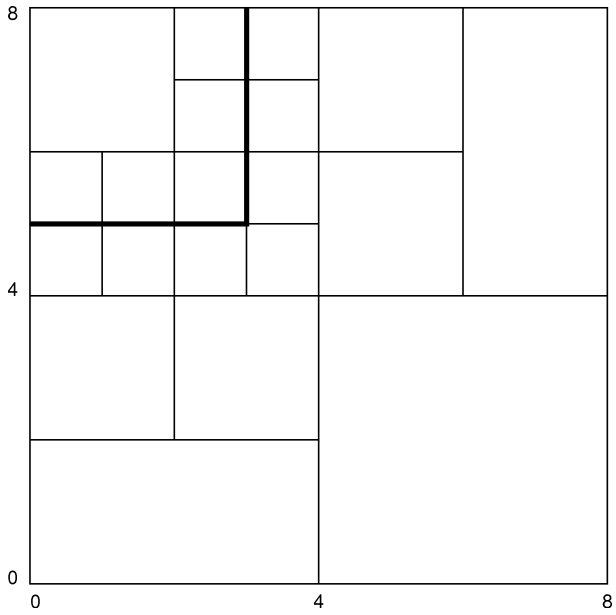

Fig. 1. A simple multiresolution mesh.

To ease the construction and subsequent navigation of the mesh, we have adopted the following constraints on cell size and abutment.

- A cell may have an aspect ratio of 1:1, 1:2, or 2:1 only.
- Adjacent cells may differ in size along a given axis by a 2:1 ratio only.
- When a cell shares an edge with a pair of neighbors, the neighbors must abut at the midpoint of that shared edge.

Fig. 1 illustrates a simple multiresolution mesh. The bold line represents a boundary between two different materials; thus, unit cells are placed there. Progressively larger cells are utilized elsewhere as permitted by the size and abutment constraints explained earlier.

A. Mesh Construction

Our method of constructing a multiresolution mesh may be summarized as follows:

1) Create unit cells along material boundaries, around localized electromagnetic sources, and anywhere else within the model space that one wishes to maximize the accuracy of current density estimates.
2) For each region in which border cells have not yet been assigned a specific material, make this assignment via a trace of all the borders that enclose, or exist within, the region.
3) Fill all conductive regions with cells of maximum size.

The details of mesh construction vary, depending upon the form of input we are given. There are two different forms of input we want to accommodate: a prediscretized model (for example, a digitized representation of a medical X-ray), or a model

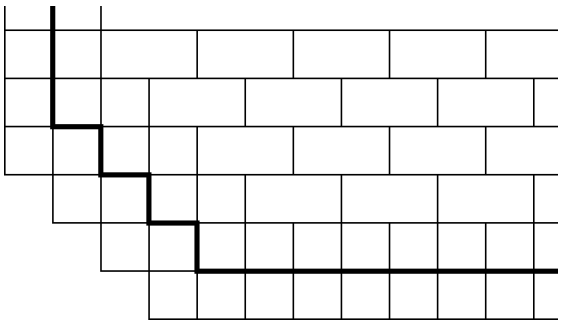

Fig. 2. An illustration of the bricking phenomenon.

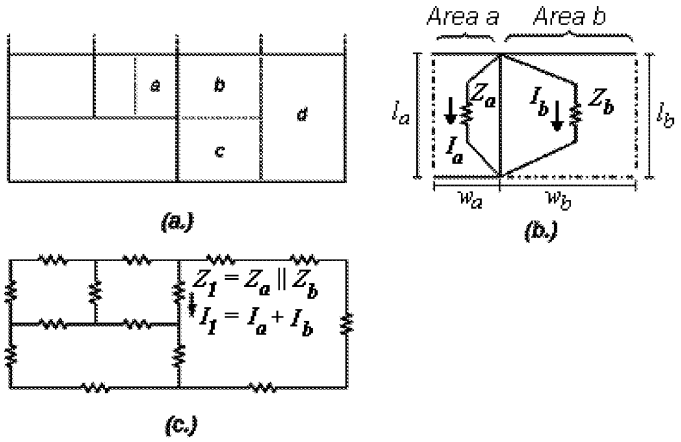

Fig. 3. (a) The lower half of the simple multiresolution mesh of Fig. 1. (b) Detail of cells a and b used for the computation of the impedance on the boundary between the two cells and (c) the complete impedance network.

described geometrically (for example, a 2-D model described in terms of straight lines and arcs).

A prediscretized model is fit to a uniform grid, and typically the input is a file of small integers. An integer's position in the file corresponds to a cell's location in the model, and the integer's value denotes the material present at that cell location. Given such a model, Step 1 of mesh construction may be performed simply by scanning the input file in search of integer pairs that correspond to adjacent cells of differing materials. Given a geometric description of a model, Step 1 is accomplished by using standard algorithms (see, for example, [7]) to map the geometric entities to an orthogonal grid. In either case, though, these processes are not directly tied to the representation or subsequent use of the mesh, so we omit further discussion of them here.

Step 2 applies only when a model (or a portion thereof) is described geometrically. With this form of input, materials are not assigned to cells when they are created in Step 1. After the first step is complete and, thus, all regions are fully defined, "region locators" are used to link materials to specific locations. Such locators must be provided for each bounded region in the model. Each region is explored outward from the locator coordinate, and every border that is discovered is traced so that its cells may be assigned to the region material.

When filling regions, we could, in theory, place a cell at any location, subject to the size and abutment constraints described earlier. The risk is that a region may be filled in a wasteful manner, as illustrated in Fig. 2. This "bricking" effect is avoided by adopting the following cell placement restriction: We place a cell of size $s_x \times s_y$ only at locations $\langle x, y \rangle$ that satisfy $|x - c_x| \ mod \ s_x = |y - c_y| \ mod \ s_y = 0$, where $\langle c_x, c_y \rangle$ is some chosen reference point.

We use a simple iterative algorithm to perform Step 3. The algorithm has the following three phases.

1) Fill each row with 2×2, 2×1, 1×2, and 1×1 cells, choosing the largest cells allowed by the placement constraint just described (in this step, there is no danger of violating the size and abutment constraints).
2) Iterate over the rows, combining adjacent cells where all constraints permit, until no more combinations are possible. Note that we may combine two rectangular cells to create a square cell, or we may combine two square cells to create a rectangular one.

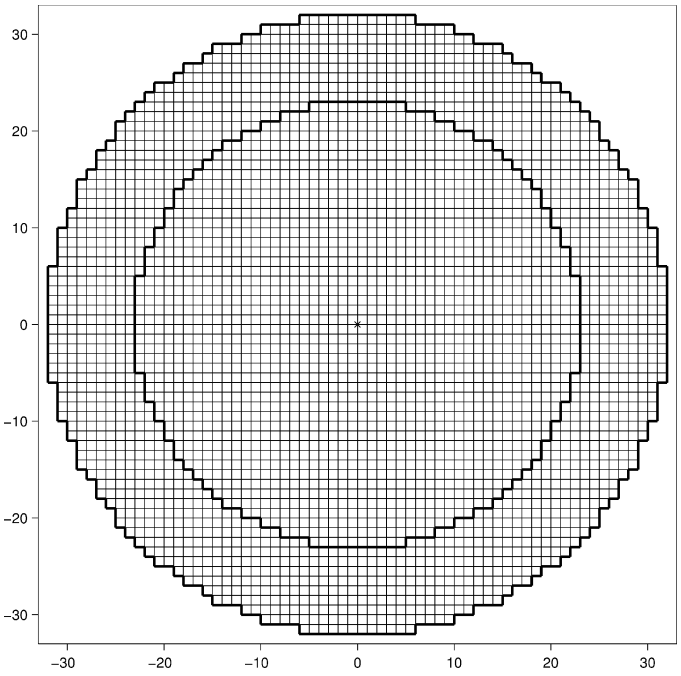

Fig. 4. The concentric cylinder model after uniform discretization (3228 cells).

3) Iterate over the rows, combining adjacent cells without regard to the placement constraint (the size and abutment constraints must still be respected, of course), until no more combinations are possible.

III. Derivation of the Impedance Network and Associated Current Densities

Derivation of the impedance network is conceptually no different with a multiresolution mesh than with a uniform mesh, in that each lumped impedance is derived from portions of two adjacent cells. To illustrate, Fig. 3 shows the lower half of the simple multiresolution mesh of Fig. 1 and its corresponding impedance network. In a straightforward extension of the calculation used in the case of a uniform mesh, impedance Z_1 in

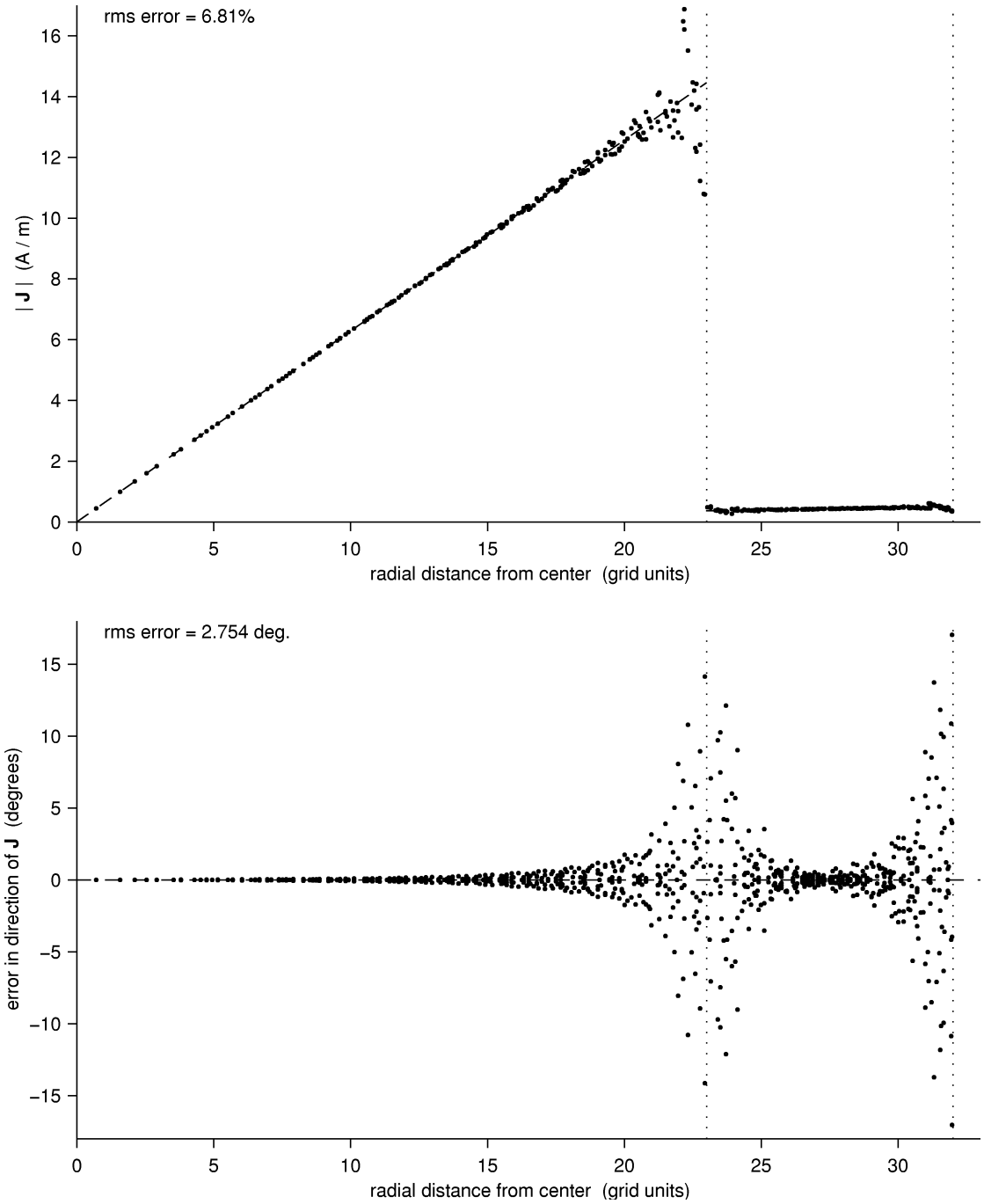

Fig. 5. Simulation results for the uniform mesh of Fig. 4.

Fig.3 (b) is derived from the half-cell a and the quarter-cell b in Fig.3 (a) using the formula

$$Z_1 = Z_a || Z_b = \frac{1}{\frac{1}{\frac{l_a}{w_a}\rho_{a_y}} + \frac{1}{\frac{l_b}{w_b}\rho_{b_y}}} = \frac{1}{\frac{2}{\rho_{a_y}} + \frac{1}{\rho_{b_y}}} \qquad (1)$$

After the network is subjected to the desired stimulus and the branch currents are obtained, current densities are computed by appropriately dividing each branch current between the two cell parts comprising the branch impedance, and then using the dimensions and properties of the cell parts to convert from current to current density. For example, having found branch current I_1 in Fig.3 (b), the current density in the quarter-cell b would be computed as

$$J_b = \frac{I_b}{w_b} = \left(\frac{Z_a}{Z_a + Z_b} I_1\right) \frac{1}{w_b} \qquad (2)$$

In the case of a uniform mesh, each cell will have a pair of current density estimates for each axis. These are typically reduced to a single current density estimate by averaging the pair of current density values for each axis, thus obtaining a vector-valued current density estimate (nominally located at the centroid of

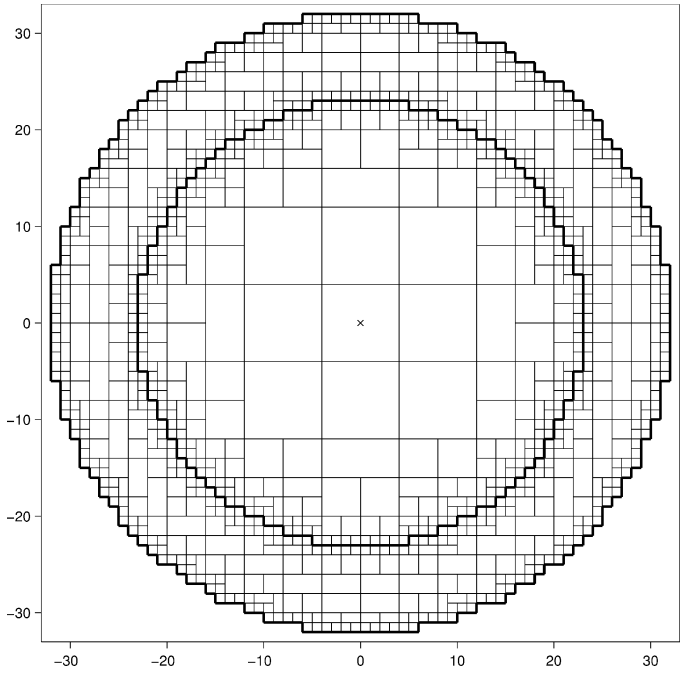

Fig. 6. The concentric cylinder model after multiresolution discretization (1101 cells).

the cell). In a multiresolution mesh, a cell may have two, three, or four current density values for a given orientation (axis), but they may still be reduced to a single value in the obvious manner. For example, current density values for cell parts b, c, and d would be reduced to a single value

$$J_{\text{cell}_y} = \frac{\frac{J_b + J_c}{2} + J_d}{2}. \tag{3}$$

IV. Link With SPICE

Since the physical model is represented by a network of lumped elements, it is possible to augment the network with passive and active lumped elements in order to model complex electrical excitations and biological responses. A circuit simulator such as SPICE is then used to solve the enhanced network.

To permit the use of these enhanced models, we have extended our mesh generator so that it can output a SPICE netlist representing the impedance network. Additional lumped elements are then added to this netlist. An important consequence is the possibility of including a variety of source conditions that are difficult to combine in a single method; any combination of voltage and current sources can be included with only small modifications to the mesh generator's internal data structures and algorithms employed to derive the impedance network. Equally attractive is the capability of introducing complex electrical lumped elements without additional modifications to the method. Voltage and current controlled sources, capacitors, and so on can be used to model bioelectrical responses.

V. Results

The goal of multiresolution meshing is to achieve a substantial reduction in the number of cells (or, more precisely, the number of branch currents) without an excessive reduction in accuracy. In this section, we evaluate the performance of our method to ascertain our success in meeting this goal.

A. Accuracy

A verification of the accuracy will ideally involve a model for which an analytical solution is obtainable. The concentric cylinder test case used by Gandhi *et al.* in [1] is, therefore, used here. It consists of a pair of concentric cylinders surrounded by free space, with material properties chosen to approximate muscle tissue ($\sigma = 0.4$ S/m) in the inner cylinder and fat ($\sigma = 0.01$ S/m) in the region between the cylinders. The inner cylinder is 23 cm in diameter, and the outer one is 32 cm in diameter. Air surrounds the model and, therefore, there is no need to discretize the region beyond the outer cylinder. In [1], a 0.5-cm-square cell was employed; we also use this as our unit cell. The incident radiation is a 1 MHz, 10^{-4} tesla magnetic field directed along the positive z axis.

For this example, we have chosen to use only the simple resistivity $\rho = 1/\sigma$, rather than the more general complex resistivity $\rho = 1/(\sigma + j\omega\varepsilon)$. The analytical solution for this model is as follows: Given a cylindrical object of conductivity σ, and a magnetic flux density B (of radian frequency ω) oriented perpendicular to that object, the expected current density at a distance r from the object's centroid has a magnitude given by

$$|\mathbf{J}| = \frac{1}{2} r\omega B_z \sigma \tag{4}$$

Thus, in our specific case, the current density should be zero at the origin, increase linearly to a maximum of 14.45 A/m^2 at $r = 11.5$ cm, drop abruptly to a value of 0.36 A/m^2, increase linearly again to a maximum of 0.50 A/m^2 at $r = 16$ cm, and then drop abruptly to zero. The current flow should be perfectly concentric about the centroid of the model; that is, it should be perpendicular to any radial line anchored at the centroid.

To quantitatively summarize the deviation of our computed magnitudes from the ideal, we compute the root-mean-square (rms) value of the percentage error. For each data point, the percentage error is computed as

$$J_{\text{err}_i} = \frac{\left| J_{\text{ideal}_i} - J_{\text{computed}_i} \right|}{J_{\text{ideal}_i}} \tag{5}$$

and the rms error is then computed as

$$J_{\text{rms}} = \sqrt{\sum J_{\text{err}_i}^2} \tag{6}$$

To summarize the deviation of the computed current flow direction, we compute the rms value of the deviation in degrees from the ideal value as

$$J_{\text{err}_i}^{\circ} = \left| J_{\text{ideal}_i}^{\circ} - J_{\text{computed}_i}^{\circ} \right| \tag{7}$$

and then compute the rms error as above.

Uniform and multiresolution discretizations of the concentric cylinder model are shown in Figs. 4 and 6, respectively. To establish a baseline for comparison, we first obtain the current density at the centroid of each cell in the uniform discretization; the results are shown in Fig. 5. We observe good agreement with theoretical values, except near the material interface. (The existence of relatively large errors where materials of substantially different conductivities meet is an artifact of the stairstep discretization of the material interface. This phenomenon has been studied in [8].)

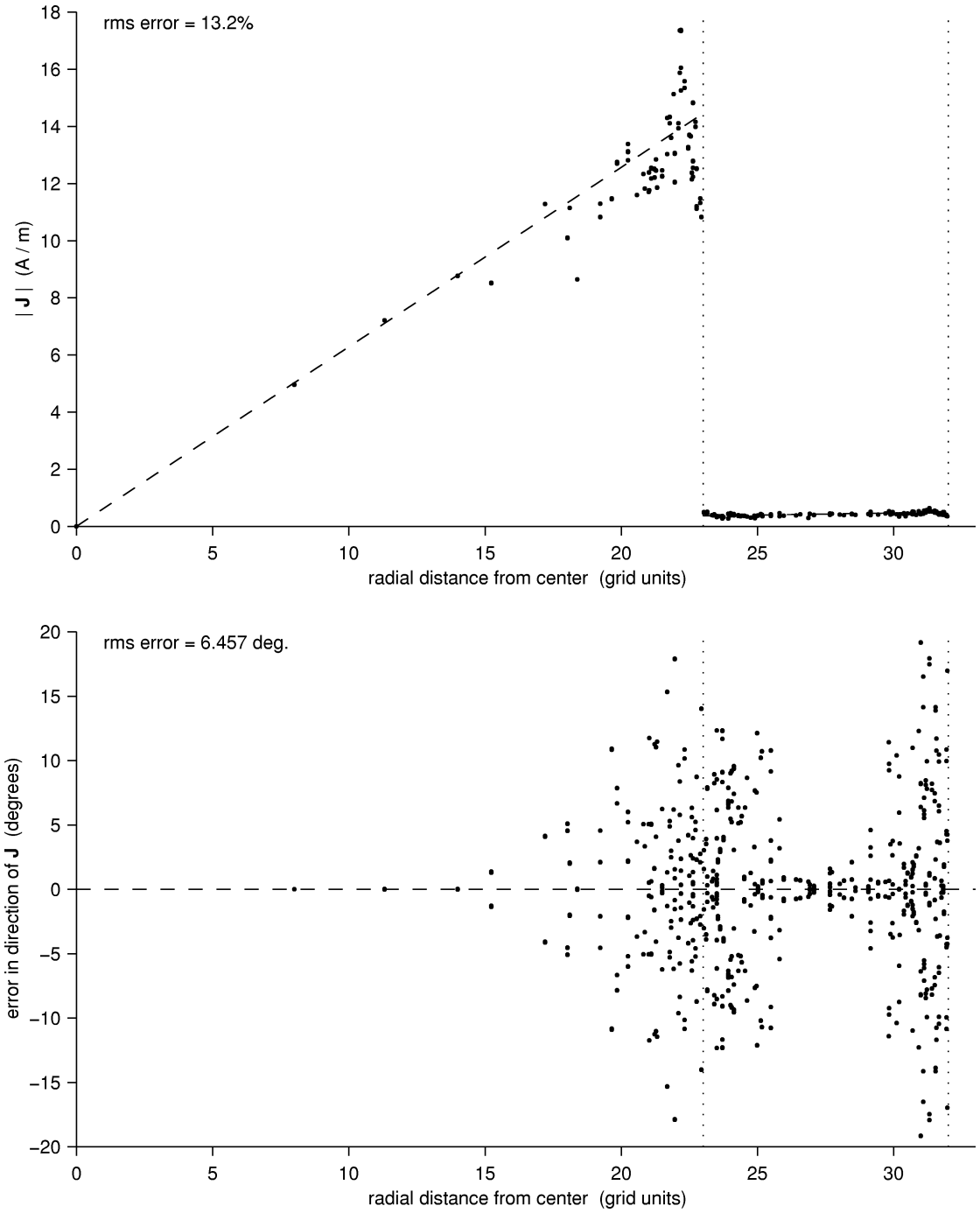

Fig. 7. Simulation results for the multiresolution mesh of Fig. 6.

Our results for the multiresolution mesh of Fig. 6 appear in Fig. 7 (again, data points correspond to cell centroids). For both the current density magnitude and direction, the distribution of data points for the multiresolution grid has the same overall pattern as for the uniform grid: The widest scattering occurs just inside the perimeter of the inner cylinder. In other words, the scattering of data points is not strongly correlated with cell size; instead, it remains strongly correlated with the proximity to material interfaces. The rms error has increased by a factor of about 1.9 for the magnitude, and by a factor of about 2.3 for the direction.

B. Reduction in Cell Count and Solution Time

The impedance method finds natural application in bioelectromagnetic studies, but the use of high-resolution discretized models has been hindered by the computational burden they impose. For example, we have taken a magnetic resonance image and digitized it to a resolution of 0.25 mm (that is, a unit cell is 0.25 mm on a side); this yields a discretized model with 670×861 cells. Of these 576 870 cells, 421 657 represent conductive material; the resulting linear system of 421 657 equations has 1 682 052 off-diagonal coefficients.

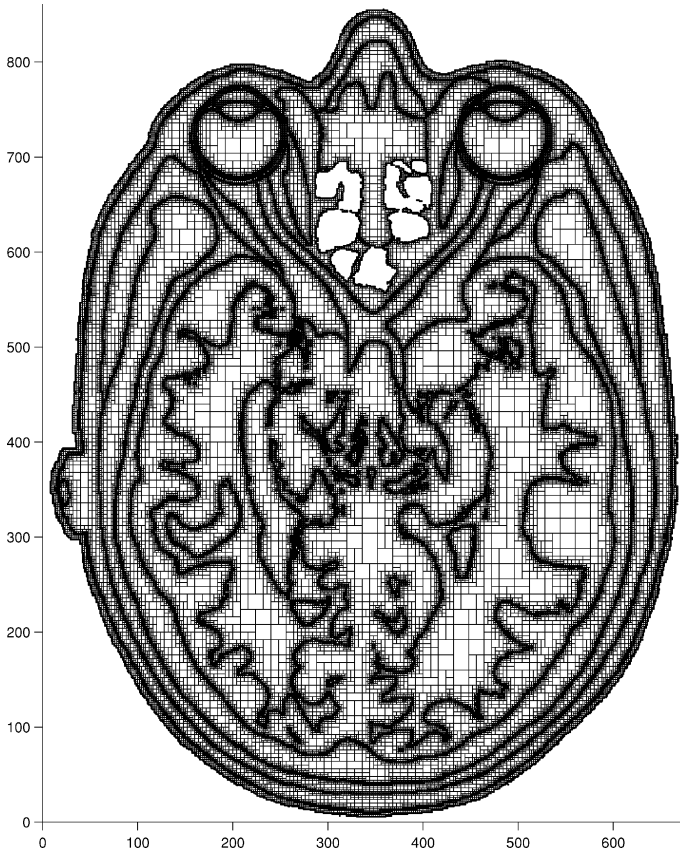

Fig. 8. A skull cross section after multiresolution discretization. Overall dimensions are 670 × 861.

TABLE I
NORMALIZED CPU TIMES FOR A SIMULATION OF THE SKULL CROSS SECTION IN FIG. 8

	mesh construction	linear system construction and solution ($\omega = 1.985$)	Total
uniform mesh	1	641	642
multiresolution mesh	123	94	217

Fig. 8 shows the results of applying our multiresolution meshing scheme to the discretized model. Only 102 411 cells are needed to fill the conductive material, and the resulting linear system has 446 830 off-diagonal coefficients: This is a 76% reduction in loop equations and a 73% reduction in off-diagonal coefficients. Table I illustrates the benefit of these reductions: Overall, the multiresolution mesh brings a 66% reduction in execution time for this example. (We solved the linear systems using the successive over-relaxation method, with a relaxation factor of 1.985.) It should also be noted that a mesh is typically generated once and then used in multiple simulation runs. In this case, once the mesh is generated, the multiresolution impedance method actually achieves an 85% reduction in execution time.

To illustrate the potential for practical biomedical applications of the method, the current spread in a retina stimulated by contact electrodes (necessary for the development of a retinal prosthesis to restore partial vision to the blind) is computed.

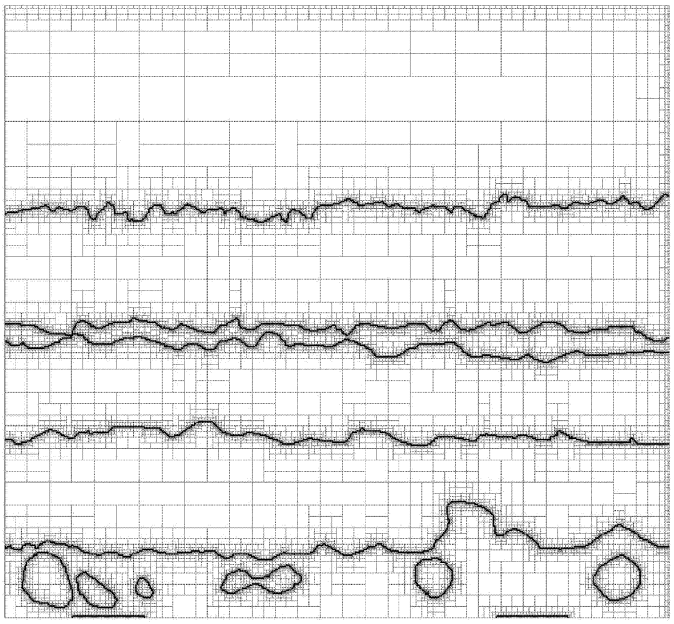

Fig. 9. A human retina after multiresolution discretization. The two dark lines along the bottom of the mesh represent epiretinal electrodes.

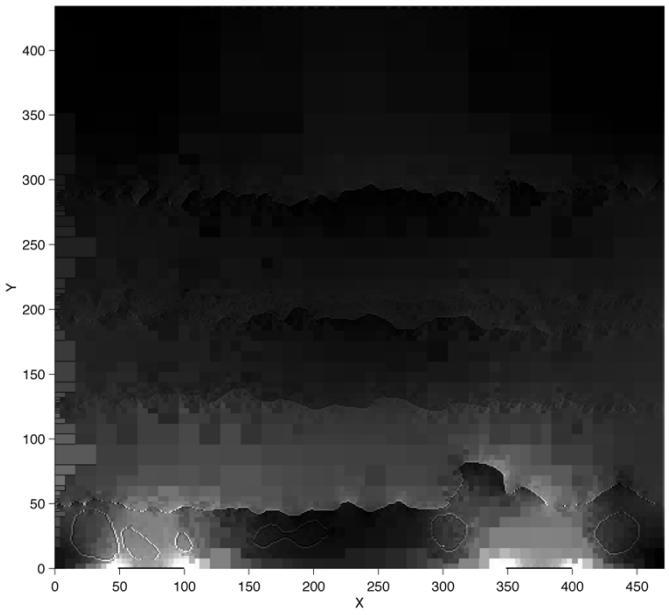

Fig. 10. The computed current density for the multiresolution mesh of Fig. 9 when the epiretinal electrodes are used as a current source.

Significant reductions of computer memory and computational time are achieved with the multiresolution discretization of the human retina, shown in Fig. 9. The multiresolution scheme can accurately model the layered structure of the retina and its boundary using only 17 062 cells, as opposed to the 204 414 cells necessary for the uniform mesh. This represents a 92% reduction in cell count. The retina is stimulated with a pair of finite-resistance epiretinal electrodes (visible at the very bottom of the mesh) with the left electrode functioning as a current source and the right electrode as a ground, and SPICE is used to obtain the branch currents in the impedance network. Fig. 10 illustrates the resultant current density.

TABLE II
MEMORY REQUIREMENTS (IN MEGABYTES) FOR A SIMULATION OF THE SKULL CROSS SECTION IN FIG. 8

	mesh structure	sparse matrix structure (linear system)	Total
uniform mesh	0.6	38.6	39.2
multiresolution mesh	5.0	10.0	15.0

C. Memory Considerations

If our multiresolution meshing scheme is to be truly practical, significant reductions in execution time must not require unreasonable amounts of memory.

Table II summarizes the memory requirements for the head slice simulation. It is not surprising that our multiresolution mesh structure requires several times more memory than a uniform mesh: A uniform mesh can usually be represented in memory at a cost of only 1 byte/cell, while our multiresolution mesh structure requires 40 bytes/unit cell and 64 bytes/nonunit cell. However, this per-cell space penalty is muted the fact that the linear system dominates the storage requirements.

Overall, use of the multiresolution mesh reduces memory requirements by 61% for this example. We note that if we had performed the simulation with complex impedances, the linear system would occupy approximately 40% more memory, and the space required for the multiresolution mesh structure (which would not change) would become even less significant.

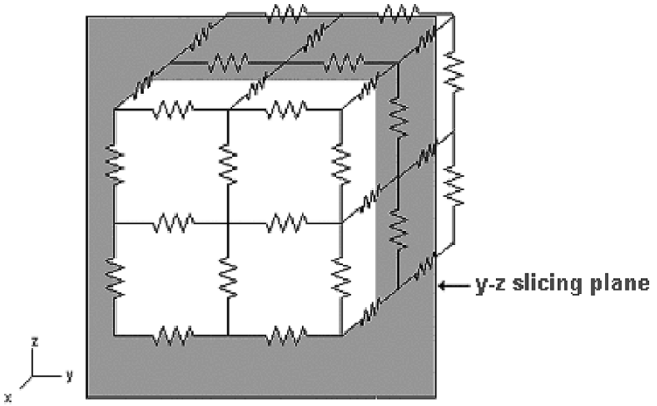

(a)

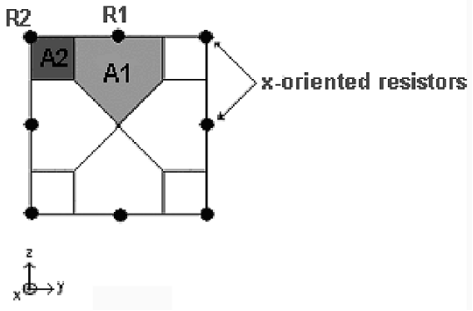

(b)

Fig. 11. (a) Example of slicing in the y–z plane to yield cross section. (b) Cross section showing the spatial orientation of x-directed resistors relative to the physical body. Each resistor accounts for the immediately surrounding area that is enclosed by the boundaries: R1 for A1, R2 for A2, and so on.

VI. EXTENSION TO THREE-DIMENSIONS

Extending the multiresolution meshing scheme to three dimensions is conceptually simple, but more complex to implement. A brief outline of the difference between the 3-D and 2-D method is presented here.

In implementing the 3-D multiresolution gridding scheme, we adhere to the same rules that we outlined in Section II for the 2-D case. No significant hurdles are encountered in the transition. However, new complexities arise in deriving the lumped impedances. For the 2-D case, the lumped impedance corresponding to a region of a cell is related to the region's length and width. A lumped impedance representing a 3-D region, however, is related to the region's length and cross-sectional area, and the cross-sectional area of a 3-D region is less obvious than the simple width of a 2-D region. For example, consider a $2 \times 2 \times 2$ cell surrounded entirely by unit cells. The central cell would have the maximum possible number of neighbors, and would contribute to 48 different resistances, as illustrated in Fig.11 (a). If that cell is halved along the y–z plane, we obtain the cross section shown in Fig.11 (b). All area in the y– z plane must be accounted for by the x-oriented impedances, but there is flexibility in the apportionment of that area among lumped impedances at the corners versus those at edge midpoints. In our 3-D approach, the cross section is divided based on proximity to cell corners and edge midpoints. In other words, if we draw lines in the x–y plane that are equidistant from the two closest x-oriented resistors, we separate the area into the appropriate sections. For the case that a cell has the maximum number of neighbors in a given plane, the cross section will be divided as shown in Fig.11 (b). When a cell has other than the maximum number of neighbors in a plane, different allocations of the cell's cross-sectional area will occur. These are not described here due to space limitations, and they will be presented in detail in a future publication.

When our 3-D multiresolution meshing scheme was applied to a discretized portion of a human eye socket, the model was reduced from 2 097 152 unit resolution cells to 1 053 123 multiresolution cells—a 50% reduction, with corresponding 50% reduction in computational time.

VII. CONCLUSIONS AND FINAL REMARKS

The impedance method is a conceptually simple numerical method for the solution of quasi-static electromagnetic problems. It is applicable in particular to many common bioelectromagnetic problems, but its use with high-resolution models has been hampered by the time required to solve the resulting system of equations. As a first step toward practical simulations, we have implemented a multiresolution 2-D mesh generation scheme for the impedance method. Our method is generally capable of reducing the number of equations to be solved by 50% to 80%, without a prohibitive increase in the space required to represent the discretized model. Where the computed results have been verified against an analytical solution, the error in

computed current density, although larger than that from a uniform mesh, remains small enough to provide useful data from the simulation.

Further, the proposed method can be linked with SPICE, thus extending the capabilities of the impedance method.

Extension of our multiresolution scheme to three dimensions is conceptually straightforward and has yielded promising preliminary results. Our success with the 2-D implementation suggests that significant computational savings may be achievable by applying a similar approach to 3-D problems.

REFERENCES

[1] O. P. Gandhi, J. F. DeFord, and H. Kanai, "Impedance method for calculation of power deposition patterns in magnetically induced hyperthermia," *IEEE Trans. Biomed. Eng.*, vol. BME-31, pp. 644–651, 1984.

[2] *ftp://starview.brooks.af.mil/EMF/dosimetry_models* [Online]

[3] D. W. Armitage, H. H. LeVeen, and R. Pethig, "Radiofrequency-induced hyperthermia: computer simulation of specific absorption rate distributions using realistic anatomical models," *Phys. Med. Biol.*, vol. 28, pp. 31–42, 1983.

[4] P. J. Dimbylow, "Induced current densities from low-frequency magnetic fields in a 2-mm resolution, anatomically realistic model of the body," *Phys. Med. Biol.*, vol. 43, pp. 221–230, 1998.

[5] T. W. Dawson, J. De Moerloose, and M. A. Stuchly, "Comparison of magnetically induced ELF fields in humans computed by FDTD and scalar potential FD codes," *Appl. Computational Electromagn. Soc. J.*, vol. 11, pp. 63–71, 1996.

[6] T. W. Dawson and M. A. Stuchly, "A comparison of analytical and numerical solutions for induction in a sphere with equatorially varying conductivity by low-frequency uniform magnetic fields of arbitrary orientation," in *Proc. 1997 Symp. Applied Computational Electromagnetics Society*, pp. 533–540.

[7] J. D. Foley, A. van Dam, S. K. Feiner, J. F. Hughes, and R. L. Phillips, *Introduction to Computer Graphics*. Reading, MA: Addison-Wesley, 1994.

[8] T. W. Dawson, M. Potter, and M. A. Stuchly, "Evaluation of modeling accuracy of power frequency field interactions with the human body," *Appl. Computational Electromagn. Soc. J.*, vol. 16, no. 2, 2001.

Michael Eberdt received the B.S.E.E. degree from Portland State University, Portland, OR, the M.S.E.E. degree from the University of Portland, Portland, OR, and the M.S.C.S. degree from North Carolina State University, Raleigh.

His primary research interest is in the area of software for electronic design and simulation.

Patrick K. Brown received the B.S. degree in electrical engineering from North Carolina State University (NCSU), Raleigh, in 2002, graduating at the top of the class. He is currently working towards the M.S. degree in electrical engineering also at NCSU.

His main research interests are in the field of interfacing electrical and biological neural systems. Specifically, he is developing novel modeling techniques to simulate electrical activity in the retina induced by stimulating electrodes.

Mr. Brown is a member of Tau Beta Pi, Phi Kappa Phi, and Phi Beta Kappa.

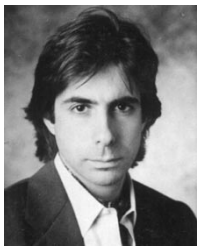

Gianluca Lazzi (S'94–M'95–SM'99) was born in Rome, Italy, on April 25, 1970. He received the Dr. Eng. degree in electronics in 1994 from the University of Rome "La Sapienza," Rome, Italy, and the Ph.D. degree in electrical engineering in 1998 from the University of Utah, Salt Lake City.

He has been consultant for several companies (1988–1994), Visiting Researcher at the ENEA (Italian National Board for New Technologies, Energy, and Environment) (1994), Visiting Researcher at the University of Rome "La Sapienza" (1994–1995), and Research Associate (1995–1998) and Research Assistant Professor (1998–1999) at the University of Utah. He is presently an Assistant Professor at the Department of Electrical and Computer Engineering, North Carolina State University, Raleigh. He is author or co-author of more than 75 international journal articles or conference presentations on FDTD modeling, dosimetry, and bioelectromagnetics.

Dr. Lazzi is the recipient of the 2003 ALCOA Foundation Engineering Research Achievement Award, a 2001 NSF CAREER Award, a 2001 Whitaker Foundation "Biomedical Engineering Grant" for Young Investigators, a 1996 International Union of Radio Science (URSI) "Young Scientist Award," and the 1996 "Curtis Carl Johnson Memorial Award" for the best student paper presented at the 18th annual technical meeting of the Bioelectromagnetics Society (BEMS). He is also an Associate Editor for the IEEE ANTENNAS AND WIRELESS PROPAGATION LETTERS. He is listed in *Who's Who in the World*, *Who's Who in America*, and *Who's Who in Science and Engineering*.